Terr. Atmos. Ocean. Sci., Vol. 27, No. 2, 203-212, April 2016 doi: 10.3319/TAO.2015.12.04.01(TT)

On Land Evidence of Ligurian Margin Normal Faults at S^t-Jean Cap-Ferrat (France)

Lionel Sonnette *

Institute of Earth Sciences, Academia Sinica, Taipei, Taiwan, R.O.C.

Received 28 July 2015, revised 3 December 2015, accepted 4 December 2015

ABSTRACT

The French Riviera has witnessed a succession of E-W trending compressions during the Oligocene period and a N-S trending compression during the Mio-Pliocene. The presence of the Ligurian Sea and drifting of the Corsica block are due to a NW-SE trending Oligo-Miocene extension. The markers of each compression are recognizable from the geological maps and they have been studied extensively in the literature. However, markers of the Ligurian Basin opening have never been described on land in the French Riviera. The structural study of the Cap-Ferrat Peninsula, at the South edge of the Nice arc, shows normal and inverse fault clusters. Their chronological relationships and the main trend of their respective stress tensors agree with the different known tectonic events and allow identification of the missing Oligo-Miocene extension on land.

Key words: Brittle tectonic, Fault, Stress tensor, French Riviera, Ligurian Basin

Citation: Sonnette, L., 2016: On land evidence of Ligurian margin normal faults at S^t-Jean Cap-Ferrat (France). Terr. Atmos. Ocean. Sci., 27, 203-212, doi: 10.3319/TAO.2015.12.04.01(TT)

1. INTRODUCTION

The French Riviera experienced a short succession of major tectonic events during the Cenozoic period. It started first with an Alpine compression responsible for the formation of N-S trending structures (Bulard et al. 1975; Gèze 1963; Ritz 1992; Laurent et al. 2000). This compression was followed by the Ligurian back-arc basin opening (Doglioni et al. 1997; Rollet et al. 2002; Sage et al. 2011). Finally a second Alpine compression marked by E-W trending thrusts (Malavieille and Ritz 1989; Ritz 1992; Laurent et al. 2000; Giannerini et al. 2011) would be responsible for setting up the Nice and Castellane arcs (Fig. 1).

Figure 1b shows the structural complexity of the Nice arc. One can identify N-S to NNW-SSE trending structures, mostly fold axis. The E-W trending structures are represented mainly by thrusts, especially at the South of the arc. Some rare cartographic examples showing the succession between the first and second Alpine compressions can also be observed:

(1) The bent N-S trending Turini synclinal (blue star on Fig. 1b) overlapped by southward thrusts at its northern border (Schreiber 2010);
(2) The Cap-Ferrat peninsula with its impressive Jurassic limestone cliff, N-S trending, and its secondary Peninsula, Cap-Ferrat Peninsula, E-W trending (red rectangle on Figs. 1b and 2; Sonnette 2012);
(3) The Malpas NW-SE trending Anticline overlapped by the southward thrust of 'Mont Agel' (red star on Fig. 1b; Giannerini et al. 2011);
(4) The Menton N-S trending Syncline overlapped by the southward thrust of S^t-Agnès (green star on Fig. 1b; Giannerini et al. 2011).

The two cross-sections in Fig. 1c illustrate the intensity and complexity of the deformation at two different Nice arc borders. Both cross-sections show thrust unit stacking with some strike-slip faults, especially for the E-W trending cross-section, which is interpreted as an Eocene-Oligocene West verging thrust reactivated as a lateral ramp accommodating the Southward motion of the Nice arc during Mio-Pliocene times (Malavieille and Ritz 1989; Ritz 1992).

The particularity of the French Riviera is the absence of any onland evidence of the Ligurian back-arc basin opening. It has been identified offshore using seismic reflexion protocols (Rollet et al. 2002; Sage et al. 2011) with a cluster of NE-SW and E-W trending normal faults and a cluster of N-S and NW-SE transfer faults. On land the only known

* *Corresponding author*
E-mail: lsonnette@earth.sinica.edu.tw

evidence is far to the West, in Provences (around Marseille) where several fault systems in syn-rift Oligocene basins have been studied using microtectonic methods (Hippolyte et al. 1993).

This paper intends to reveal the existence of some on land normal faults associated with the Ligurian extension at S^t-Jean-Cap-Ferrat, based on paleostress determination and faulting chronology in polyphased structures.

2. METHODS

2.1 Faulting Relative Chronology

It is particularly difficult to perform dating of different faults in a single geological formation, as stratigraphic correlation cannot be used. In this study, all of these faults were identified in a single undetermined Upper Cretaceous formation, post-Barremian in age (Fig. 2). All faults are either coeval or younger than this formation according to the cross-cutting relationships principle and the syn-sedimentary faulting definition. To date the different fault events (Angelier 1994) imply either:

(1) The distinction of several successive slickenside lineations on a given fault plane;
(2) The observation of crosscutting and offset relationships between successive different fault slips;
(3) The fold-test or more broadly the backtilting of the bedding in order to decipher the chronology between a tectonic event (usually a stress tensor assuming that one of the stress direction was vertical) and the tilting/folding of the bedding.

2.2 Mapping Square Decameters Areas

Tectonic maps are used to describe the fault patterns and highlight the structural relationship between the different fault clusters. No existing maps or aerial photographs

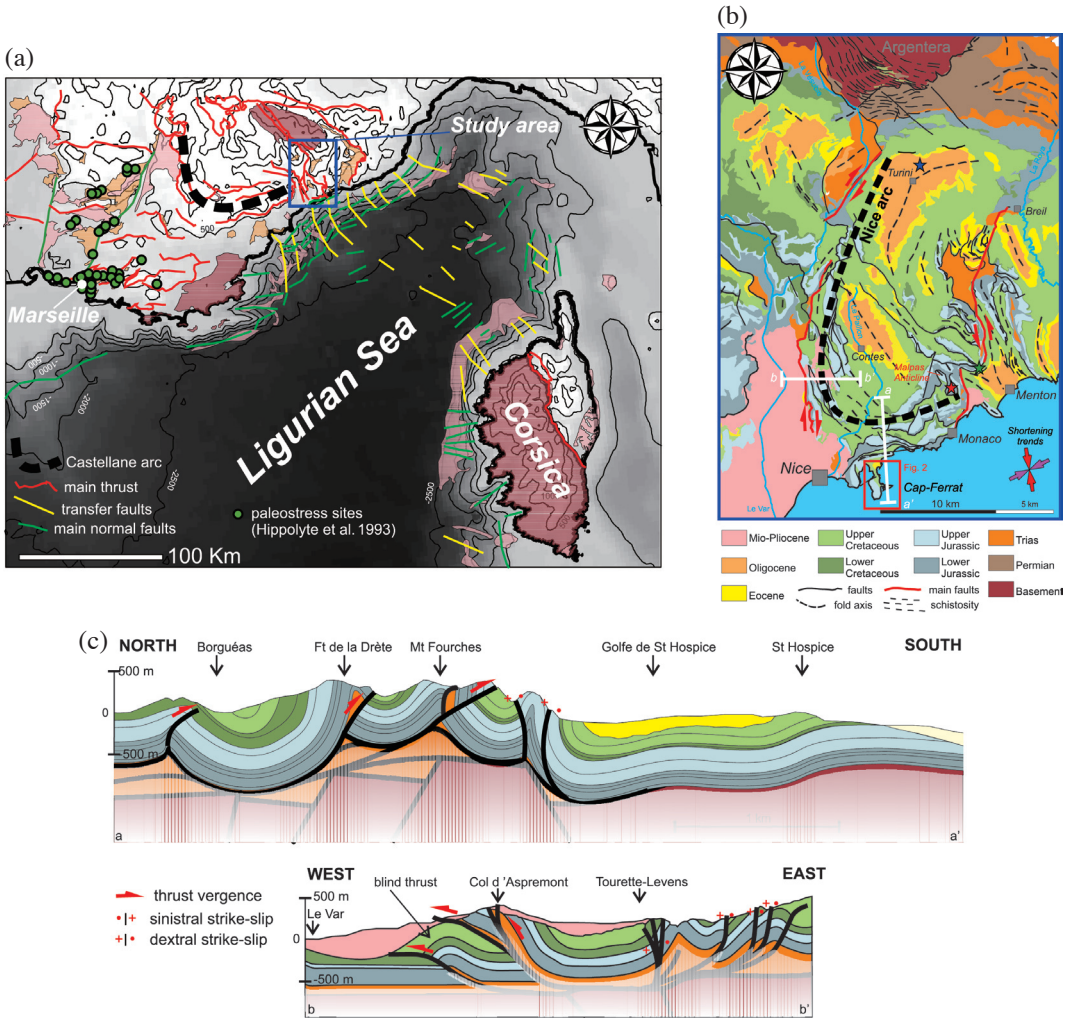

Fig. 1. (a) Synthetic structural map of the Ligurian Sea and its surroundings. (b) Simplified structural map of the Arc of Nice (modified from Gèze et al. 1957). The thrusts immediately North of Cap-Ferrat Peninsula (red rectangle) corresponds to a late N-S Alps compression whereas most of synclinals and anticlinals correspond to an old ENE-WSW compressive event (see text for references and explanations of the colored stars). (c) Two cross-sections showing the fold-fault interference between the two main compressions. (Color online only)

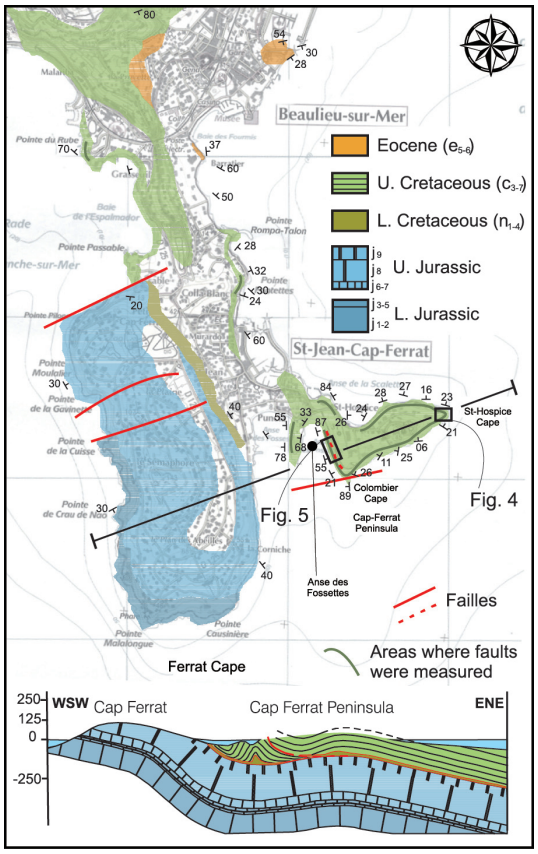

Fig. 2. Simplified geological map of the Cap-Ferrat Peninsula with the localization of the sites described in the text (rectangular frames) and a WSW-ENE cross-section showing the main structural style of the Cap-Ferrat Peninsula. The letters associated with the stratigraphic log correspond to the stage provided by the geological map of Nice-Menton (Gèze et al. 1957); j_{1-2}: Bajocian-Bathonian, j_{3-5}: Callovian-Argovian, j_{6-7}: Rauracian-Sequanian, j_8: Kimmeridgian, j_9: Portlandian, n_{1-4}: Berriasian-Barremian, c_{3-7}: Undetermined Upper Cretaceous, e_{5-6}: Lutetian-Bartonian. (Color online only)

could be use as they are not suitable for areas of several square meters only. The most reliable method (which could reach millimeter to few centimeters precision) would be to used a drone or any system capable of taking photographs at 10 - 20 m altitude. Unfortunately such devices or technology was not available. I opted for a less reliable, with a pluricentimeter-scale to pluridecimeter-scale precision, but easier method using a compass (with an inclinometer), a measuring tape (a double decameter) and a field assistant. I made the maps in polar coordinates (Fig. 3). This method can be summarized in four steps:

(1) I established a reference point (preferentially at the center of the studied areas).

(2) I measured from the reference point the azimuth and distance of different bench marks. As some tension could be applied to the measuring tape and with the support of a field assistant, I measured the dip of the measured line.

(3) Using simple trigonometry principles, I calculated the horizontal distance between each bench mark and the reference point.

(4) Finally, I drew the different fault traces and some remarkable topographic lines as the crest of some bedding layers as the elevation model could not be easily determined.

2.3 Paleostress Determination

The stress tensor calculations were made from fault slip data. Fault planes and striations orientations were used to determine the orientation of the principal stress axes σ_1, σ_2, σ_3, and the Φ ratio. The Φ ratio defines the shape of the stress ellipsoid, $\Phi = (\sigma_2 - \sigma_3)/(\sigma_1 - \sigma_3)$. I used the software 'Tector 94' developed by Professor Jacques Angelier based on the INVDIR stress inversion calculation (Angelier 1990, 2002).

3. NORMAL FAULTING AT S^t-HOSPICE CAPE

The Upper Cretaceous formation of the Cap-Ferrat Peninsula displays a brittle deformation. The geological formation is characteristic of the shelf of a continental margin with a succession of calcareous sandstone and shale layers with some preserved fossils and shell pieces. Metric to pluri-decametric normal faults are dominant. They present a striated mirror, often with oxydation, and some syntectonic calcite crystallization (Fig. 4e). A few faults show evidence of open cracks having filled by stratified yellow shale or fault breccias. Three clusters of conjugated normal faults can be distinguished according to their azimuth, respectively NW-SE, N-S, and E-W. The identification of these clusters is remarkable at the edge of the S^t-Hospice Cape where conjugated faults from each group bounds small horsts and grabens (Fig. 4a).

The faults present a unique sliding tectonic event on the fault plane. A few others present two generations of striations, usually related to an initial dip-slip normal activity and a posterior strike-slip reactivation. One fault at S^t-Hospice Cape is a very beautiful example of syntaxial calcite crystallization (Fig. 4f) with strike-slip striations on the inner fault crystallization and dip-slip striations on the border fault crystallization. The inner fault crystallization post-dates the border crystallization.

The orthogonality between the stratification surfaces and the bisector planes of the conjugated normal faults (which bound NW-SE and E-W trending grabens; Figs. 4a, c, and d) implies the posterior tilting to the North of about 20° of these structures. It is difficult to determine if N-S trending normal faults are tilted or not as their azimuths are roughly perpendicular to the identified tilt axis. Unfortunately, the tilting is too weak to precisely determine the chronology of faulting from the pitch analysis of different fault sets. Both configurations, before and after Northward tilting, are realistic and give similar directions of extension. Moreover the chronological relationship between N-S trending faults and NW-SE

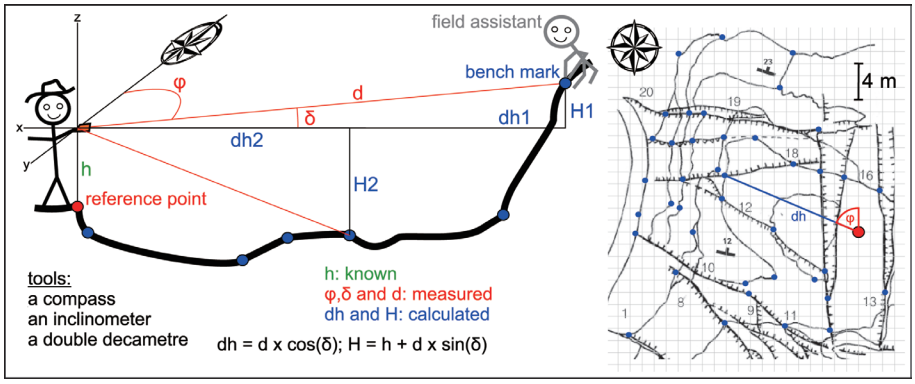

Fig. 3. Sketch explaining the mapping principles used in this study. (Color online only)

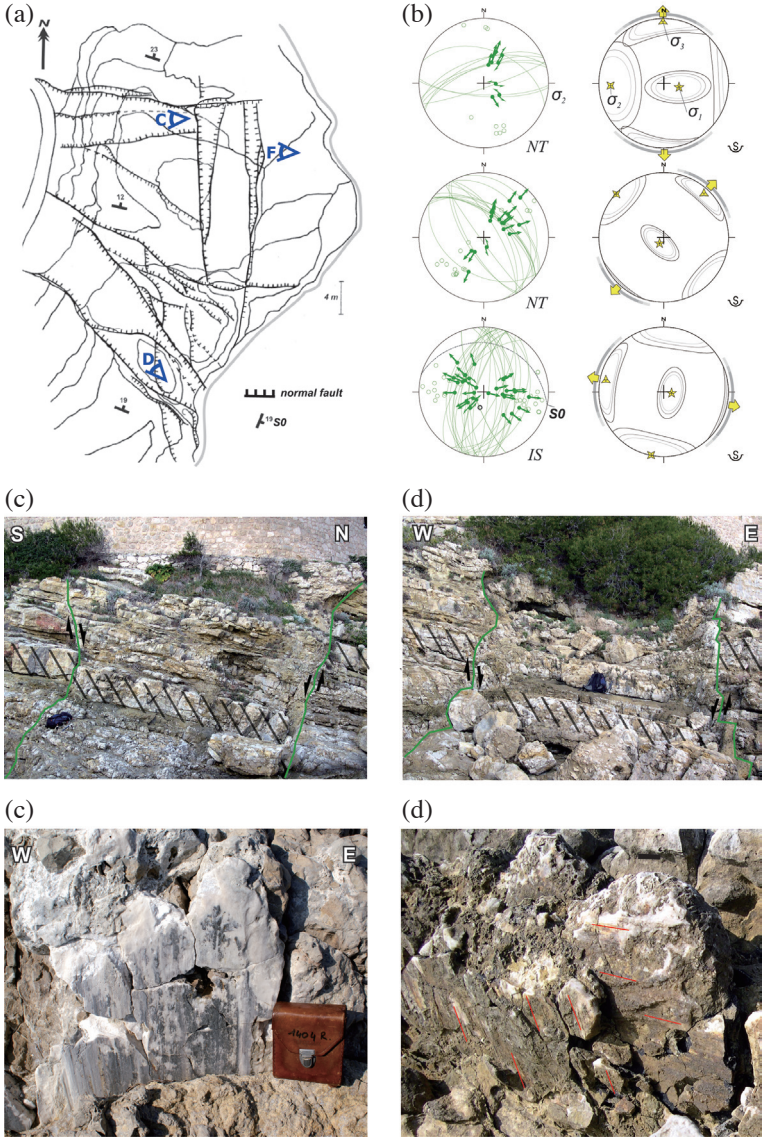

Fig. 4. (a) Detailled tectonic map of the St-Hospice Cape. (b) Results of analyses of the data after bedding correction (NT) for E-W and NW-SE trending faults and *in situ* (IS) for N-S trending faults using the inversion method. Stereographic projections of the different clusters, results by INVGLI (stress tensor calculation; Angelier 1990, 2002). Confidence ellipses are also shown for 60, 75, and 90% of confidence. The geographic and magnetic North at St-Jean-Cap-Ferrat are similar, the declination error is less than 1°. Group I and II correspond to the grouping discussed in part V: Discussion. (c), (d) Photographs of E-W and NW-SE trending grabens. (e) Example of calcite normal fault mirror, photograph taken at Colombier Cape. (f) Photograph of strike-slip and dip-slip striations on a N-S trending normal fault. Points of view of photographs C, D, and F are located on (a). (Color online only)

and E-W trending faults remains unclear as the faults cross-cut each other with no significant displacement (Fig. 4a).

I computed the corresponding stress directions for each cluster of normal faults using a stress tensor calculation method (Angelier 1990, 2002). The data and results are presented in Fig. 4b and Table 1. The computed datasets correspond to faults mapped on the S'-Hospice Cape (Fig. 4a) plus sets of normal faults measured along the eastern coast of the Cap-Ferrat Peninsula (Fig. 2). The results highlight the existence of three distinct extension events (Table 1).

(1) A NE-SW extension (σ_3: 043° ± 22 / 09° ± 10) related to NW-SE trending normal faults that formed prior to the Northward bedding tilting.
(2) A N-S extension (σ_3: 359° ± 29 / 05° ± 10) related to E-W trending normal faults, also developed before bedding tilting.
(3) An E-W extension (σ_3: 281° ± 28 / 10° ± 10) related to N-S trending normal faults whose relation with tilting could not be determined.

The chronological relationship between each normal fault cluster is unclear and could lead to the interpretation of a unique radial extensive tectonic event, with σ_1 vertical and $\sigma_2 = \sigma_3$ in the horizontal plane. However, each normal fault cluster is characterized by neo-formed conjugated systems that support successive and distinct extension episodes with various directions of extension. In a radial extension there is no specific trend for normal faulting except in the presence of an inherited fracture network. In addition, each cluster is

Table 1. Fault data and corresponding calculated tensor for each cluster of faults for S'-Hospice Cape and Colombier Cape. Fault data are presented *in situ* as follows: a quality and sense of slipping indicator (C: certainly, P: probably, S: supposed; N: normal, I: reverse, D: dextral, S: sinistral); azimuth of the fault plane; dip angle of the fault plane and the direction of dip (N, E, S, or W); pitch. Φ: ratio of the principal stresses difference, $\Phi = (\sigma_2 - \sigma_3)/(\sigma_1 - \sigma_3)$. The different tensor results are provided *in situ* or after tilting correction according to the information provided in the 'Tectonic event' column. (Color online only)

Site	Tectonic event	Data: Type Strike Dip Pitch							Tectonic regime
St-Hospice	**E-W extension**	CN 178 50E 89S	CN 175 51E 89S	CN 006 71W 75S	CN 023 60W 80N	CN 170 65E 80S	CN 015 44W 65N	CN 012 54W 82S	
	(no tilt correction)	CN 020 80W 78S	CN 005 84E 89S	CN 000 74E 86N	CN 010 66E 89N	CN 013 71W 74S	CN 018 55W 89N	CN 021 63W 85N	
		CN 175 61E 89S	CN 008 80W 86N	CN 029 73E 61N	CN 020 55E 72S	CN 002 65E 74N	CN 032 40E 84N	PN 018 46E 76S	
		CN 000 72W 70S	CN 020 79W 85S	CN 013 48W 82N	PN 018 31E 80N	CN 037 58W 70N	CN 160 78W 84S	CN 005 62W 80N	
		Calculated Tensor $\sigma_1 = 098/80°$; $\sigma_2 = 191/01°$; $\sigma_3 = 281/10°$; $\Phi = 0.46$							
	N-S extension	CN 090 58S 76E	CN 074 85N 76E	CN 074 59N 59E	CN 078 84N 89E	CN 065 62N 66E			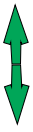
	(tilt correction, S0 107 18N)	CN 092 56S 83E	CN 110 47N 89E	CN 067 69N 71E	CN 071 84S 76E				
		Calculated Tensor $\sigma_1 = 104/70°$; $\sigma_2 = 267/19°$; $\sigma_3 = 359/05°$; $\Phi = 0.49$							
	NE-SW extension	CN 125 77N 75E	CN 125 78N 77E	CN 140 75E 64E	CN 125 77N 82E	CN 142 52E 87S	CN 125 75N 88E		
	(tilt correction, S0 107 18N)	CN 132 25S 72E	CN 138 34E 45N	CN 155 55W 70S	CN 118 66N 75E	CN 147 77E 74S	CN 125 75N 88E		
		CN 120 66N 58E	CN 125 75N 85W	CN 156 58W 66S	CN 146 72W 67S	CN 138 49E 85N			
		Calculated Tensor $\sigma_1 = 215/81°$; $\sigma_2 = 312/01°$; $\sigma_3 = 043/09°$; $\Phi = 0.49$							
Colombier	**NE-SW compression**	CI 014 25W 073	CI 163 41E 83N	CI 034 26W 070	PI 108 26N 56E	PI 140 40E 82N	CI 138 40E 80N	CI 159 45E 89N	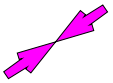
	(no tilt correction)	CI 155 31E 098	CI 116 39N 70E	CI 179 28W 073	PI 122 32E 82N	CI 170 20E 058	CI 160 38E 82N	CI 155 31E 038	
		CI 160 31E 049	CI 049 16N 070	PI 115 27N 060	PI 145 41E 72N	CI 145 36E 73N	CI 157 39E 082	PD 178 27E 074	
		Calculated Tensor $\sigma_1 = 236/10°$; $\sigma_2 = 145/00°$; $\sigma_3 = 045/80°$; $\Phi = 0.53$							
	N-S extension	CN 064 63S 86E	CN 066 68S 82W	CN 083 54S 86E	CN 085 66S 56E	PN 117 49N 80E	CN 113 58N 89E	CN 052 52S 82E	
	(no tilt correction)	CN 062 69S 72E	CN 076 47S 86W	PN 088 54N 89E	CN 091 54S 82E	PN 116 56N 53E	PN 090 68N 87E	CN 055 47S 81E	
		CN 077 78S 70E	CN 078 51S 78E	CN 095 37N 89E	CN 082 50S 85W	PN 085 26N 51W	CN 080 66N 87W	CN 060 43S 83E	
		Calculated Tensor $\sigma_1 = 345/81°$; $\sigma_2 = 252/01°$; $\sigma_3 = 162/09°$; $\Phi = 0.42$							

very well defined mechanically with a Φ ratio around 0.5, which means that the stress magnitude ratio between σ_3 and σ_2 and between σ_2 and σ_1 are equal and therefore not supporting any kind of stress permutation.

4. RELATIVE CHRONOLOGY OF FAULTING AT COLOMBIER CAPE

The Cap-Ferrat Peninsula is also affected by folds, reverse and strike-slip faults. These features can be observed at Colombier Cape (Fig. 2). The range of reverse fault azimuths is between N115°E and N195°E, and the dipping range is between 20 - 40° (usually South - Westward). Their azimuths are not appreciable in Fig. 5a because the dip of reverse faults plunge in the same direction as the topographic slope (Fig. 5c). Regarding strike-slip faults, they range from N135°E to N-S trending and they cut through all of the other reverse and normal faults. Both the sinistral and dextral sense were determined but no clear conjugate fault system can be identified. Normal faults are also present, with only E-W trends and similar fault characteristics described at the S'-Hospice Cape. Although the bedding dip increases

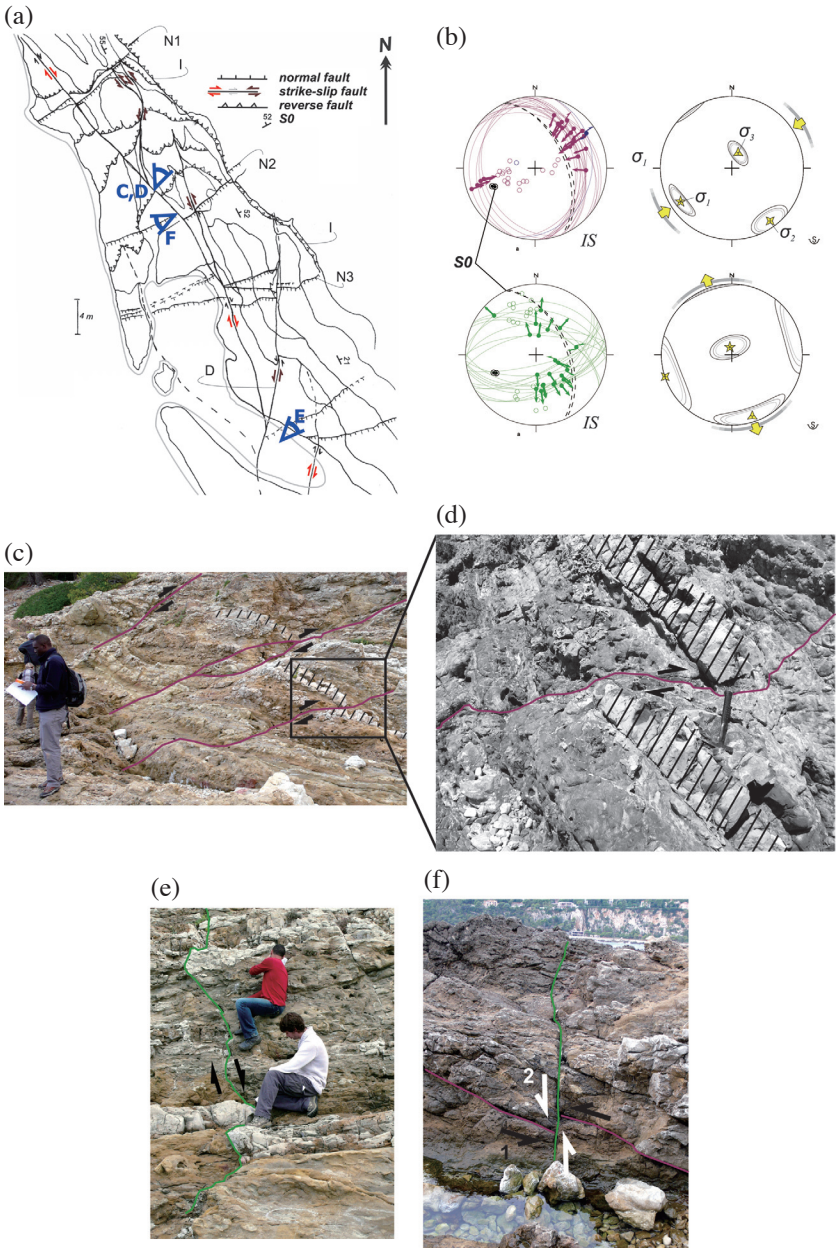

Fig. 5. (a) Detailled tectonic map of the Colombier Cape. (b) Results of analyses of the data inversion method. Stereographic projections of the different clusters, results by INVGLI (stress tensor calculation; Angelier 1990, 2002). Same legend as Fig. 4. (c), (d) Example of reverse fault, zooming in on a cut limestone layer. (e) Example of a normal fault, whose offset can be appreciated at the feet of the two students. (f) Chronological relationship between reverse and normal faults. Points of view of photographs C, D, and F are located on (a). (Color online only)

Northward (Figs. 2 and 5) the fault clusters, normal and reverse, do not display large discrepancies in the studied area. None of these features are affected by the NNW-SSE trending folds of the western part of the Cap-Ferrat Peninsula (Fig. 2), because they are younger than the folding.

Reverse faults (Figs. 5c and d) are clearly crosscut by E-W trending normal faults (Fig. 5f), except one (labelled I on Fig. 5a) which is parallel to the stratification and seems to crosscut the E-W trending normal faults. The apparent gap is sinistral (see fault N1, N2, and N3 on Fig. 5a). However, near fault I, the normal faults end in a network of horse tail fractures. On the reverse fault plane I, the pitch of the striations imply a dextral apparent offset of the normal faults. These observations suggest that the fault would have acted as a transfer zone rather than a fault posterior to normal faulting. An alternative interpretation would be to consider a sinistral strike-slip reactivation of reverse fault I based on a sinistral fault connection (between N2 and N3 on Fig. 5a). The apparent offsets of normal faults are all similar in the 0.5 - 1 m range. However, as no strike-slip second generation of striations have been identified along reverse fault I, the first interpretation is preferred, in relation to the décollement of the Cretaceous layers over the Jurassic limestones (Fig. 2b).

A detailed analysis of the NNW-SSE trending fold forming the Colombier Cape and the 'Anse des Fossettes' highlights 16° Northward plunge (Fig. 6). The fold axis trend suggests folding during ENE-WSW horizontal shortening, whereas its Northward plunge could indicate a later tilting related to a N-S oriented shortening or just the effect of some fold interference during the ENE-WSW trending folding.

In light of a potential northward Colombier Cape tilting, the tectonic analysis (inversion calculation, Fig. 5b and Table 1) was also carried out after applying a tilt correction. The correction does not optimize the position of the maximum and minimum stress along the vertical for reverse and normal fault clusters respectively. The reverse and normal faults therefore probably postdate the tilting to the ENE due to folding and the Northward tilting of the fold. The results presented on Fig. 5b are *in situ* with no bedding tilt correction applied. Reverse faults reveal their compatibility with an ENE-WSW compression (σ_1: N236°E ± 12 trending 10° ± 5 dipping) which is in agreement with the development of NNW-SSE trending folds. E-W trending normal faults are consistent with a NNW-SSE extension (σ_3: N162°E ± 20 trending 9° ± 5 dipping). The dataset is not exclusive to the mapped area in Fig. 5 and includes some faults measured all along the coastline of the Cap-Ferrat Peninsula (Fig. 2).

In summary, the Colombier Cape outcrop highlights the following tectonic history:

(1) Folding followed by faulting consistent with a ENE-WSW compression;
(2) Normal faulting consistent with a N-S extension;
(3) Strike-slip faulting consistent with a NW-SE compression.

5. DISCUSSION: DO NORMAL FAULTS REFLECT MARGIN EXTENSION?

The different fault clusters along the Cap-Ferrat Peninsula have been described and the corresponding stress tensors calculated. I will argue in the following paragraphs how I interpret these different clusters according to the different known tectonic events from Cretaceous time to the Present for the Nice area.

5.1 Plio-Quaternary Strike-Slip Faulting

On Cap-Ferrat Peninsula, strike-slip faults cut through all of the other structures, faults and folds. Commonly, N-S and NW-SE trending normal faults are respectively with sinistral and dextral sense at Colombier Cape or reactivated with sinistral and dextral sense at S't-Hospice Cape. Strike-slip faults seems to be consistent in general with a NW-SE compression. The corresponding stress inversion is not presented due to the lack of reliable measurements

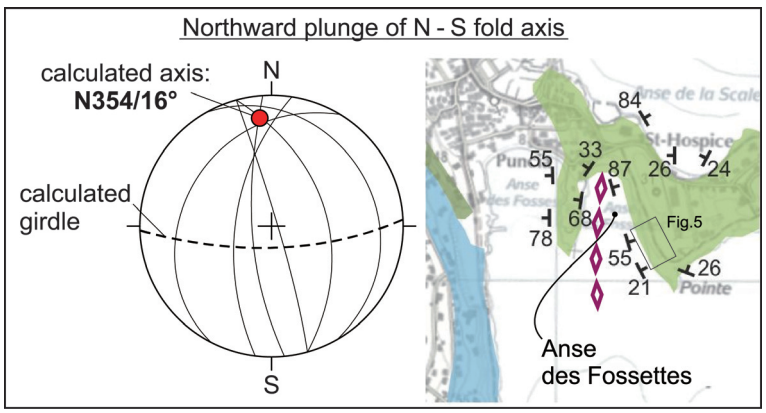

Fig. 6. Northward plunge of the fold NNW-SSE axis of the Colombier Cape and location of map displays in Fig. 5. (Color online only)

(less than 10 faults). Moreover, the sense of strike-slipping is usually difficult to establish and one can note in Fig. 5a the co-existence of faults with similar azimuths but with opposite slipping direction. These features correspond either to two tectonic events perpendicular to each other, or to a unique tectonic event in which the compression direction varys across a large range of azimuths about a NNW-SSE average. In both cases, strike-slip faults are not compatible with either reverse or normal faults and appear to post-date them. As these faults are posterior to all other structural features they could only be formed during the most recent tectonic regime which is the Pliocene to Present N-S to NW-SE trending compression (Nocquet and Calais 2004; Bauve et al. 2012).

5.2 Oligocene Reverse Faulting and Folding

The reverse fault cluster is consistent with an ENE-WSW compression. N-S trending folds forming the Cap-Ferrat cape and the Colombier cape are also consistent with such compression (Fig. 2). The ENE-WSW compression is consistent with the NE-SW to E-W trending compressive event that affected the region during Oligocene (Gèze 1963; Bulard et al. 1975; Ritz 1992). Reverse faults are evidence of the Oligocene compression prior to Ligurian Sea rifting.

5.3 Oligo-Miocene E-W Trending Normal Faults

The S'-Hospice and Colombier Cape E-W trending normal faults clusters are consistent with a N-S extension. Their chronological relationship with folding and reverse faulting highlights their occurrence after the ENE-WSW compression. The structural analysis of these two places highlights the interpretation of a Northward tilt for the whole Cap-Ferrat Peninsula, which could be the response to Southward Nice Arc thrusting during the Mio-Pliocene periods (Ritz 1992; Giannerini et al. 2011), especially at the S'-Hospice Cape. This N-S extension occurred between an Oligocene ENE-WSW compression and a Mio-Pliocene Northward tilt. Chronologically these faults are very good candidates for accommodating the Ligurian extension on land. In addition, these faults present a certain compatibility with the on land evidence in Provence (Hippolyte et al. 1993) and the numerical modelling results (Carminati et al. 1998) of the NW-SE Ligurian Basin opening (Doglioni et al. 1997; Rollet et al. 2002), which is accommodated offshore by E-W trending normal faults (Sage et al. 2011). These normal faults are evidence on land of the Oligo-Miocene extension.

5.4 NW-SE Trending Normal Faults

The S'-Hospice Cape NW-SE trending normal fault cluster is consistent with a NE-SW extension. This cluster predates the bedding tilting to the North but there is no evidence of their timing relative to the ENE-WSW compression. Did they occur prior to this folding phase or synchronous with the subsequent N-S extension? Whatever, the only correlation I have found with the literature is some compatibility with the N015-045°E extension proposed by Hippolyte et al. (1993) in Provence for latest Rupelian and early-middle Chattian. In Provence this extension is significantly different from the expected N-S and NW-SE Ligurian Sea extension, and interpreted as the interaction between the West-European rifting and the Ligurian sea opening. They could be potential on land evidence of the Oligo-Miocene extension or a late Cretaceous unknown extension.

5.5 N-S Trending Normal Faults

The N-S trending normal fault S'-Hospice Cape cluster is consistent with an E-W extension. The relation with the bedding tilt and with the ENE-WSW compression are unclear. Other studies in Lower Cretaceous outcrops (Hibsch et al. 1992; Montenat et al. 1997) in the Nice and Castellane Arcs revealed that the only known tectonic regimes are an E-W trending Valanginian extension and a post-Barremian strike-slip event (σ_1 is sub-meridian and σ_3 is mostly E-W trending). The post-Barremian tectonic regime could be consistent with the E-W extension determined at S'-Hospice Cape. The implications of such interpretation are that the N-S trending normal fault cluster predates the ENE-WSW compression and the post-Barremian event was effective during the Upper Cretaceous period, which correspond to the age of the Cap-Ferrat Peninsula formations. The N-S trending normal faults could also be related to the last stage of the Ligurian Sea opening, as proposed in the numerical modelling at 16/15 and 9/8 Ma from Carminati et al. (1998); which proposed that once the Corsica-Sardinia block separated from the continent, the extension trended mainly E-W, precursory to the Tyrrhenian Sea opening. These normal faults could be potential on land evidence of the Oligo-Miocene extension or a post-Barremian extension.

Although there are some dating ambiguities, especially related to the ENE-WSW compression, which allow a wide range of interpretations, the consideration of a previously not recognized extension event from the Upper Cretacecous period to Present; it is interesting to notice that it is possible to explain all normal fault clters with the support of Carminati et al.'s numerical modeling (1998) from 21 to 9/8 Ma and the interpretation of Hippolyte et al. (1993). Indeed for the studied area location, the extension direction evolve from N150°E ± 10 to N095°E ± 5 in their models. Such evolution in the extension direction could explain the imbrication of the E-W and N-S trending grabens at the S'-Hospice Cape and the difficulty in distinguishing any relative chronology. Normal Cap-Ferrat Peninsula faults would be evidenced on land at the Ligurian Sea margin extension.

6. CONCLUSION

The Cap-Ferrat Peninsula is located at the boundary between the allochthonous thrusts of the Nice arc and the autochthonous Ligurian continental margin (Recq et al. 1976). From the offshore seismic reflexion profile study, Sage et al. (2011) interpreted tilted blocks bounded by major E-W trending normal faults. Cap-Ferrat Peninsula outcrops reveal a remarkably complete history of regional Cenozoic period deformation. One can clearly distinguish Alpine compressive tectonic events and several normal faulting. The E-W trending normal faults developed after the first Alpine E-W compression and they are related to a N165°E ± 21 trending extension consistent with the known Ligurian Basin opening direction (N155°E for the Chattian period according to Hippolyte et al. 1993). These faults are the first evidence on land of the Ligurian Sea opening along the French Riviera. Further works will be to perform some dating on the brecchia and the sedimentation filling some inter-fault spaces. It will be interesting to look after paleostress evidence in Corsica and Sardinia in order to perform a complete analysis of the stress field associated with the Ligurian Sea opening.

Acknowledgements I deeply thank Profs. Jacques Angelier and Bertrand Delouis (UMR 7329 Géoazur, UNS-CNRS-IRD-OCA) for giving me such an interesting topic during my undergraduate formation that I could continue working on during my Ph.D. This study was part of some undergraduate work completed during my Doctorate thesis at the University of Nice Sophia-Antipolis. I thank Dr. Cédric Legendre and Dr. Romain Plateaux for taking the time to read the present work at the initial stage of preparation. I also thank Prof. Domingo Aerden for his comments and suggestions in improving this manuscript. I am grateful to Academia Sinica for providing me a postdoc fellowship, so that completion of this manuscript would be possible. This is a contribution of the Institute of Earth Science, Academia Sinica (IESAS 1981). This work was also supported by MOST (Ministry of Science and Technology) of Taiwan, under grant No. MOST 104-2116-M001-020.

REFERENCES

Angelier, J., 1990: Inversion of field data in fault tectonics to obtain the regional stress--III. A new rapid direct inversion method by analytical means. *Geophys. J. Int.*, **103**, 363-376, doi: 10.1111/j.1365-246X.1990.tb01777.x. [Link]

Angelier, J., 1994: Fault-slip analysis and paleostress reconstruction. In: Hancock, P. L. (Ed.), Continental Deformation, Pergamon, Oxford, 101-120.

Angelier, J., 2002: Inversion of earthquake focal mechanisms to obtain the seismotectonic stress IV--A new method free of choice among nodal planes. *Geophys. J. Int.*, **150**, 588-609, doi: 10.1046/j.1365-246X.2002.01713.x. [Link]

Bauve, V., Y. Rolland, G. Sanchez, G. Giannerini, D. Schreiber, M. Corsini, J. L. Perez, and A. Romagny, 2012: Pliocene to Quaternary deformation in the Var Basin (Nice, SE France) and its interpretation in terms of "slow-active" faulting. *Swiss J. Geosci.*, **105**, 361-376, doi: 10.1007/s00015-012-0106-4. [Link]

Bulard, P. F., B. Chamagne, G. Dardeau, J. Delteil, P. Gioan, J. P. Ivaldi, F. Laval, J. L. Pérez, and J. Polvêche, 1975: Sur la genèse et les structures de l'Arc de Nice. *B. Soc. Geol. Fr.*, **XVII**, 939-944, doi: 10.2113/gssgfbull.S7-XVII.6.939. [Link]

Carminati, E., M. J. R. Wortel, P. T. Meijer, and R. Sabadini, 1998: The two-stage opening of the western-central Mediterranean basins: A forward modeling test to a new evolutionary model. *Earth Planet. Sci. Lett.*, **160**, 667-679, doi: 10.1016/S0012-821X(98)00119-8. [Link]

Doglioni, C., E. Gueguen, F. Sàbat, and M. Fernandez, 1997: The Western Mediterranean extensional basins and the Alpine orogen. *Terr. Nova*, **9**, 109-112, doi: 10.1046/j.1365-3121.1997.d01-18.x. [Link]

Gèze, B., 1963: Caractères structuraux de l'arc de Nice (Alpes-Maritimes). Mémoires Hors Série de la Société Géologique de France, 289-300.

Gèze, B., M. Lanteaume, Y. Peyre, J. Vernet, and W. Nestero, 1957: Carte géologique de la France au 1/50000, feuille Menton-Nice.

Giannerini, G., G. Sanchez, D. Schreiber, J. M. Lardeaux, Y. Rolland, A. B. de Castro, and V. Bauve, 2011: Geometry and sedimentary evolution of the transpresssive Roquebrune-Cap Martin basin: Implications on the kinematics and timing of the Nice arc deformation during Miocene times, SW Alps. *B. Soc. Geol. Fr.*, **182**, 493-506, doi: 10.2113/gssgfbull.182.6.493. [Link]

Hibsch, C., D. Kandel, C. Montenat, and P. O. d'Estevou, 1992: Evenements tectoniques crétacés dans la partie méridionale du bassin subalpin (massif Ventoux-Lure et partie orientale de l'arc de Castellane, SE France); implications géodynamiques. *B. Soc. Geol. Fr.*, **163**, 147-158.

Hippolyte, J. C., J. Angelier, F. Bergerat, D. Nury, and G. Guieu, 1993: Tectonic-stratigraphic record of paleostress time changes in the Oligocene basins of the Provence, southern France. *Tectonophysics*, **226**, 15-35, doi: 10.1016/0040-1951(93)90108-V. [Link]

Laurent, O., J. F. Stephan, and M. Popoff, 2000: Modalités de la structuration miocène de la branche sud de l'arc de Castellane (chaînes subalpines méridionales). *Géologie de la France*, **3**, 33-65.

Malavieille, J. and J. F. Ritz, 1989: Mylonitic deformation of evaporites in décollements: Examples from the southern Alps, France. *J. Struct. Geol.*, **11**, 583-590, doi: 10.1016/0191-8141(89)90089-8. [Link]

Montenat, C., C. Hibsch, J. C. Perrier, F. Pascaud, and P. de Bretizel, 1997: Tectonique cassante d'âge crétacé inférieur dans l'Arc de Nice (Alpes-Maritimes, France). *Géologie Alpine*, **73**, 59-66.

Nocquet, J. M. and E. Calais, 2004: Geodetic measurements of crustal deformation in the Western Mediterranean and Europe. *Pure Appl. Geophys.*, **161**, 661-681, doi: 10.1007/s00024-003-2468-z. [Link]

Recq, M., J. P. Rehault, G. Bellaiche, M. Gennesseaux, and J. P. Esteve, 1976: Unites structurales de la marge continentale sous-marine de Cannes a Menton d'apres la sismique refraction. *Earth Planet. Sci. Lett.*, **28**, 323-330, doi: 10.1016/0012-821X(76)90193-X. [Link]

Ritz, J. F., 1992: Tectonique récente et sismotectonïque des Alpes du Sud: Analyses en termes de contraintes. *Quaternaire*, **3**, 111-124, doi : 10.3406/quate.1992.1980. [Link]

Rollet, N., J. Déverchère, M. O. Beslier, P. Guennoc, J. P. Réhault, M. Sosson, and C. Truffert, 2002: Back arc extension, tectonic inheritance, and volcanism in the Ligurian Sea, Western Mediterranean. *Tectonics*, **21**, 6-1-6-23, doi: 10.1029/2001TC900027. [Link]

Sage, F., M. O. Beslier, I. Thinon, C. Larroque, J. X. Dessa, S. Migeon, J. Angelier, P. Guennoc, D. Schreiber, F. Michaud, J. F. Stephan, and L. Sonnette, 2011: Structure and evolution of a passive margin in a compressive environment: Example of the south-western Alps-Ligurian basin junction during the Cenozoic. *Mar. Petrol. Geol.*, **28**, 1263-1282, doi: 10.1016/j.marpetgeo.2011.03.012. [Link]

Schreiber, D., 2010: Modélisations géométriques 3D et champs de déformations dans les Alpes du Sud. Ph.D. Thesis, Université de Nice Sophia-Antipolis, 306 pp.

Sonnette, L., 2012: Etude structurale et paléomagnétique de la courbure des systèmes plissés et chevauchants des arcs de Nice, de Castellane et du Nord-Est de Taiwan. Ph.D. Thesis, Université de Nice Sophia-Antipolis, 337 pp.